Simulation of a liquid propellant rocket engine manufacturing assembly line utilizing the PFS/PN methodology

Eduardo Seiji Suguimoto Miyazato Ferrer, Jhonatan Ribeiro dos Santos

Abstract – The system addressed in this paper pertains to an assembly line for liquid propellant rocket engines equipped with turbopump. The challenge involves automating the process of metal 3D printing for the turbopump and combustion chamber, followed by heat treatment for stress relief, X-ray computed tomography inspection, and the subsequent movement of components throughout the factory. To achieve this, the PFS/PN methodology was employed to facilitate a detailed analysis of the system, ensuring control over its inputs and outputs. The system was simulated using the *ProModel* Discrete Event Simulator, and the results were scrutinized, indicating the robustness of the simulation. Following the Ladder methodology, programming for Programmable Logic Controllers was also developed.

Palavras-chave – Liquid Propellant Rocket Engine; Discrete Event System; Metal Additive Manufacturing; Industry 4.0

1 Introduction

In recent years, the aerospace industry has undergone a significant revolution in the conception, design, and manufacturing of critical components for spacecraft. Particularly, metal 3D printing has emerged as a pioneering technology, redefining the traditional boundaries of conventional manufacturing. This transformation is especially evident in the sector of liquid rocket engines, where the implementation of metal 3D printing not only promises to optimize production processes but also to redefine the efficiency, sustainability, and scalability of the space industry.

The fundamental importance of this innovation lies in its ability to overcome intrinsic challenges in the conventional production of liquid rocket engines. The geometric complexity of these engines, coupled with stringent requirements for strength and durability, historically imposed substantial limitations on traditional manufacturing, leading to the production of a single engine taking weeks to months (BAO et al, 2022). However, metal 3D printing offers a revolutionary approach, enabling the creation of intricate components with complex geometries, such as injectors (3D SYSTEMS, 2020) (BAO et al, 2022), turbopumps (BAO et al, 2022), and regeneratively cooled chambers (MORIYA et al, 2018) (BAO et al, 2022) (3D SYSTEMS, 2020), while maintaining exceptional levels of strength and reliability, reducing manufacturing time to less than a week (BAO et al, 2022), and costs to less than 20%, due to reduced labor and material and energy waste (BAO et al, 2022).

Versão inicial submetida em 27 de dez. de 2023. Versão final aceita em 28 de dez. de 2023. Publicado emem 28 de dez. de 2023. Digital Object Identifier 10.11606/issn.2526-8260.mecatrone.2023.221035

Furthermore, the use of 3D printing allows the integration of various components into one, reducing the number of system components and interfaces, thereby enhancing reliability while reducing manufacturing time and labor requirements (SALMI, 2019)(BAO et al, 2022). Moreover, in the current space landscape characterized by a growing private industry presence, the increasing importance of metal 3D printing in achieving ambitious goals is highlighted. Private space companies such as SpaceX, Relativity Space, Rocket Lab, and Blue Origin(BAO et al, 2022) have stood out globally, driven by a unique combination of innovation, flexibility, and operational efficiency (SALMI, 2019). In this context, the ability to manufacture liquid rocket engines using metal 3D printing technology emerges as a crucial competitive advantage, enabling these companies to explore new space frontiers in an agile, economical, and sustainable manner (BAO et al, 2022). In March 2023, the US-based company Relativity Space successfully launched the world's first 3D-printed orbital rocket (SALMI, 2019).

This article aims to automate a liquid rocket engine assembly line to make the entire process more cost-effective, faster, and scalable.

2 Methodology

2.1 The Discrete Event System concept

Discrete Event Systems (DES) represent a category of dynamic systems in which state changes occur at specific moments in response to discrete events. The literature underscores the significance of these systems in modeling processes that evolve in discrete steps, highlighting applications in industrial automation, traffic control, and communication protocols.

2.2 Behavioral model using modeling techniques

Behavioral modeling in discrete event systems often employs techniques such as Petri Nets. These nets provide a powerful graphical representation to visualize interactions between events and states. The PFS/PN methodology (Petri Nets and Functional Specifications/Petri Nets), proposed by (MIYAGI, 1996), combines the flexibility of Petri Nets with detailed functional specifications, offering a comprehensive approach for modeling and analyzing discrete dynamic systems.

2.3 The IEC 61131-3 standard for programming

The IEC 61131-3 standard, an international standard for the programming of Programmable Logic Controllers (PLCs), plays a crucial role in the landscape of industrial automation. Developed by the International Electrotechnical Commission (IEC), this standard establishes fundamental guidelines for software creation in automation environments.

Furthermore, the standard emphasizes software portability, enabling programs to run on different PLCs from various manufacturers as long as they adhere to IEC 61131-3. This not only simplifies hardware integration but also promotes efficient code reuse through standardized libraries.

Regarding programming languages, IEC 61131-3 offers five options, spanning from graphical diagrams such as the Ladder Diagram (LD), inspired by electrical schematics, to high and low-level languages like Structured Text (ST) and Instruction List (IL).

2.4 Transcription of RdP into programming language

The transcription of Petri net-based models into programming languages is a crucial step in the practical implementation of discrete event systems. For the transcription process, the ladder language was employed. Within this language, the methodology presented in the classroom setting was adhered to, encompassing the sequential activation of transitions, places, and outputs with their respective addressing. To achieve this, it is imperative to have previously constructed the Petri net, associating each signal (internal and external) to ensure the faithful representation of the system's operation in the diagram.

2.5 Project Methodology

Initially, the adopted methodology involved mapping all projects of interest that could be analyzed in discrete events. Once the project was chosen, the execution of the PFS became necessary. Upon obtaining the results, the PIPE software was used to generate the Petri net (RDP) for the project, creating transitions and places for each specific action of the activity. Simultaneously, *ProModel* was employed to verify the project's operation, providing a visual understanding of the processing behavior. With the RDP created, inputs and outputs were associated with it, and corresponding addressing for each was established. Following the addressing and association, the methodology for ladder programming was implemented. Thus, with the obtained data, it was possible to thoroughly examine the project's properties, ensuring comprehensive validation.

3 Application of Mechatronic Automation

3.1 Description of the system to be automated (schematic model).

The model to be automated consists of an assembly line for liquid rocket engines. This process can be observed in Figure 1.

Figure 1 - Assembly line diagram

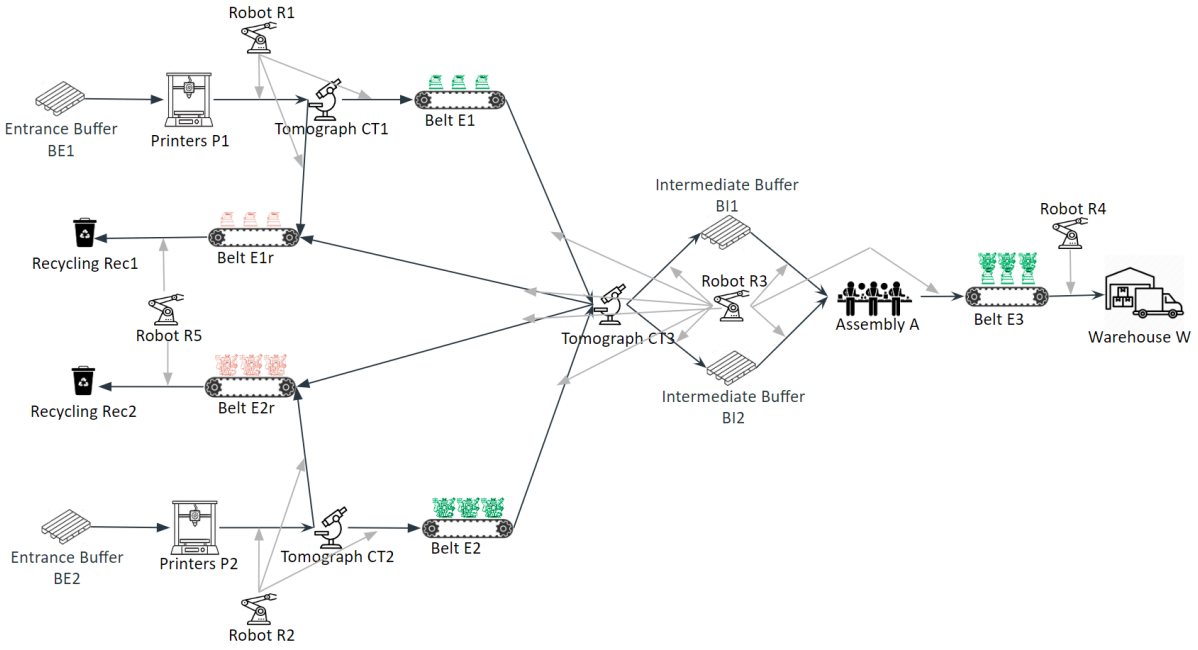

3.2 Structural Model of the System

In printing bay 1, there are 9 3D Direct Energy Deposition Laser printers (L-DED) (P1s) for printing the combustion chamber and nozzle system. This technology, among various existing ones (YUSUF et al, 2019) (GRADL et al, 2019), achieves the fusion of a metallic filament at the tip of a

robotic arm. It is ideal for printing large parts that do not require extremely high geometric resolution (BLAKEY-MILNER et al, 2021) (BECK et al, 2020). This is because it does not necessitate a large reservoir with metallic powder, and the dimension is only limited by the reach of the print head. The selected material for these components is the Copper-Chromium-Zirconium alloy for the internal layer of the chamber, due to its high thermal conductivity and resistance to high temperatures, and Inconel 768 for the external layer, due to its high mechanical strength (MORIYA et al, 2018). Once the component is printed, a robotic arm (R1) transports it to an X-ray computerized tomography machine (CT2), which is one of the primary inspection methods for components manufactured by 3D printing. This machine allows the verification of the existence of any cracks, pores, trapped residues, warping, and other defects (BLAKEY-MILNER et al, 2021) (SOLLER and ARIANE, 2015).

If the component is approved, it is transported by the robotic arm (R1) to the conveyor belt (E1) of the furnace (F), where the removal of residual stresses is carried out through heating (BLAKEY-MILNER et al, 2021) (MORIYA et al, 2018). (The removal of any metallic residues before heat treatment is recommended but will not be done for system simplification). This furnace operates continuously, ensuring that parts enter and exit continuously through the movement of the conveyor belt (E1). Otherwise, the piece is discarded by the robotic arm (R1) to the recycling conveyor (E1r), which transports the piece to the recycling bay 1 (Rec1), where it will be transformed back into metallic filament, ready to be fed back into the printer (P1). This part of the process will not be addressed in this work.

In printing bay 2, there are 12 3D Laser Powder Bed Fusion (L-PBF) printers (P2s) (BLAKEY-MILNER et al, 2021) for printing the powerhead (SOLLER and ARIANE, 2015) and turbopump. This technology is suitable for printing complex systems that require high precision, allowing multiple pieces to be printed simultaneously (BLAKEY-MILNER et al, 2021) (REI, 2018). This is due to the precise laser fusion process of metallic powder, where the powder itself below the fusion region serves as a support for the part (YUSUF et al, 2019). The materials used for these components are Inconel 718 and Stainless Steel 316-L, chosen for their high mechanical strengths and corrosion resistance (SOLLER et al, 2018). Again, once the component is printed, a robotic arm (R2) transports it to a computerized tomography machine (CT2) for part inspection, aiming to detect possible cracks or bubbles in the material, as well as the location of metallic powder between the newly printed components. If the component is approved, it is transported by the robotic arm (R2) to the conveyor belt (E2), where manual removal of metallic powder between the components is performed (MORIYA et al, 2018). Otherwise, the piece is discarded by the robotic arm (R2) to the recycling conveyor (E2r), which transports the piece to the recycling bay 2 (Rec 2), where it will be transformed back into metallic powder, ready to be fed back into the printer (P2).

Once both sets of mentioned components are completed, they are transported to the computerized tomography equipment (CT3), where the final inspection of these components is carried out. If approved, they are transported to the assembly bay (A) by the robotic arm (R3), where manual assembly takes place. If rejected, they are transported by the robotic arm (R3) to the recycling conveyors 1 or 2, which takes the rejected components to the recycling bays.

Subsequently, the complete engine is transported to the conveyor belt (E3), which carries it to the warehouse, where it is unloaded by the robotic arm (R4) and stored. Later, it will be loaded onto a transport vehicle for delivery to the customer. This part of the process will not be addressed in this work.

3.3 Application of Modeling Methodology

A Representation of Processes in PFS (Production Flow Schema)

The first step of the methodology is to represent the main processes in a diagram, as can be seen in Figure 2.

Figure 2 - Representation of processes in PFS.

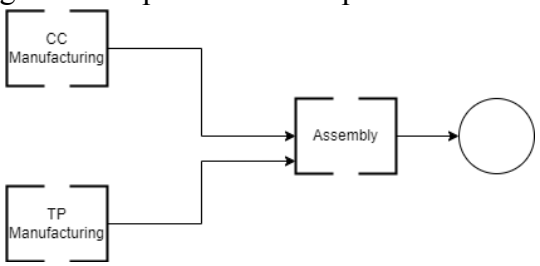

B Detailed Processes within PFS Activities

The second step is to split each process into the activities, using the desired level of details, represented at Figure 3.

Figure 3 - Activities in PFS.

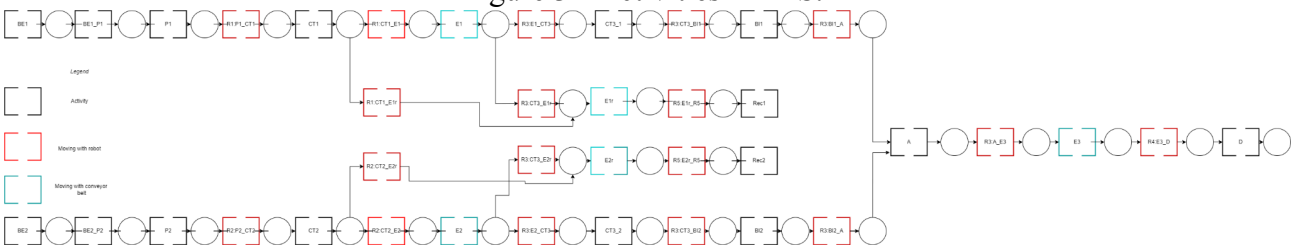

In the present case, the process can be detailed into the following activities:

- **BE1**: Arrival of metallic filament at Entrance Buffer 1;
- **BE2**: Arrival of metallic powder at Entrance Buffer 2;
- **BE1_P1**: Loading into Printer 1;
- **BE2_P2**: Loading into Printer 2;
- **P1**: Printing of combustion chamber by Printer 1;
- **P2**: Printing of turbopump by Printer 2;
- **CT1**: Inspection on Computerized Tomography Equipment 1;
- **CT2**: Inspection on Computerized Tomography Equipment 2;
- **CT3_1**: Inspection of the chamber on Computerized Tomography Equipment 3;
- **CT3_2**: Inspection of the turbopump on Computerized Tomography Equipment 3.
- **BI1**: Arrival of combustion chambers at Intermediate Buffer 1;
- **BI2**: Arrival of turbopumps at Intermediate Buffer 2;
- **A**: Assembly of parts;
- **D**: Storage of parts in the warehouse.
- **Rec1**: Arrival of defective chambers at the recycling bay;
- **Rec2**: Arrival of defective turbopumps at the recycling bay;
- **R1:P1_CT1**: Movement from P1 to CT1 through robot 1;
- **R1:CT1_E1**: Movement from CT1 to E1 through robot 1;
- **R1:CT1_E1r**: Movement from CT1 to E1r through robot 1;
- **R2:P2_CT2**: Movement from P2 to CT2 through robot 2;
- **R2:CT2_E2**: Movement from CT2 to E2 through robot 2;
- **R2:CT2_E2r**: Movement from CT2 to E2r through robot 2;

- **R3:E1_CT3**: Movement from E1 to CT3 through robot 3;
- **R3:CT3_BI1**: Movement from CT3 to BI1 through robot 3;
- **R3:CT3_E1r**: Movement from CT3 to E1r through robot 3;
- **R3:BI1_A**: Movement from BI1 to A through robot 3;
- **R3:E2_CT3**: Movement from E2 to CT3 through robot 3;
- **R3:CT3_BI2**: Movement from CT3 to BI2 through robot 3;
- **R3:CT3_E2r**: Movement from CT3 to E2r through robot 3;
- **R3:BI2_A**: Movement from BI2 to A through robot 3;
- **R3:A_E3**: Movement from A to E3 through robot 3;
- **R4:E3_D**: Movement from R3 to D through robot 4;
- **R5:E1r_R1**: Movement from E1r to Rec1 through robot 5;
- **R5:E2r_R2**: Movement from E2r to Rec2 through robot 5.
- **E1**: Movement through conveyor belt 1;
- **E2**: Movement through conveyor belt 2;
- **E3**: Movement through conveyor belt 3;
- **E1r**: Movement through conveyor belt 1r, to the recycling area;
- **E2r**: Movement through conveyor belt 2r, to the recycling area.

C Elaboration of Activities Detailing the Introduction of Petri Net Elements

Then, the PFS can be translated into a Petri Net, where the circles represent a location and the bars, transitions, as depicted in Figure 4.

Figure 4 - Activities and movements in PN.

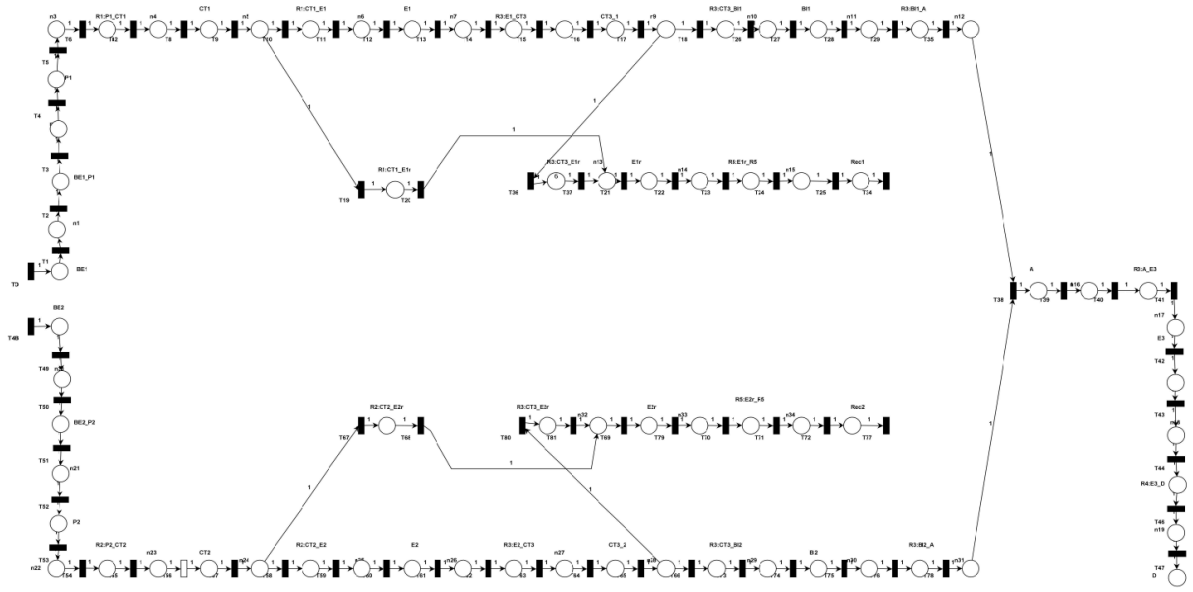

D Introduction of Resource Control Elements for Sharing

Resources that are shared between more than one activity, such as printers, robots and tomography equipments need to be carefully analysed, since they can performed one task at a time.

Figure 5 - Activities and movements in PFS with Resouce Control Elements.

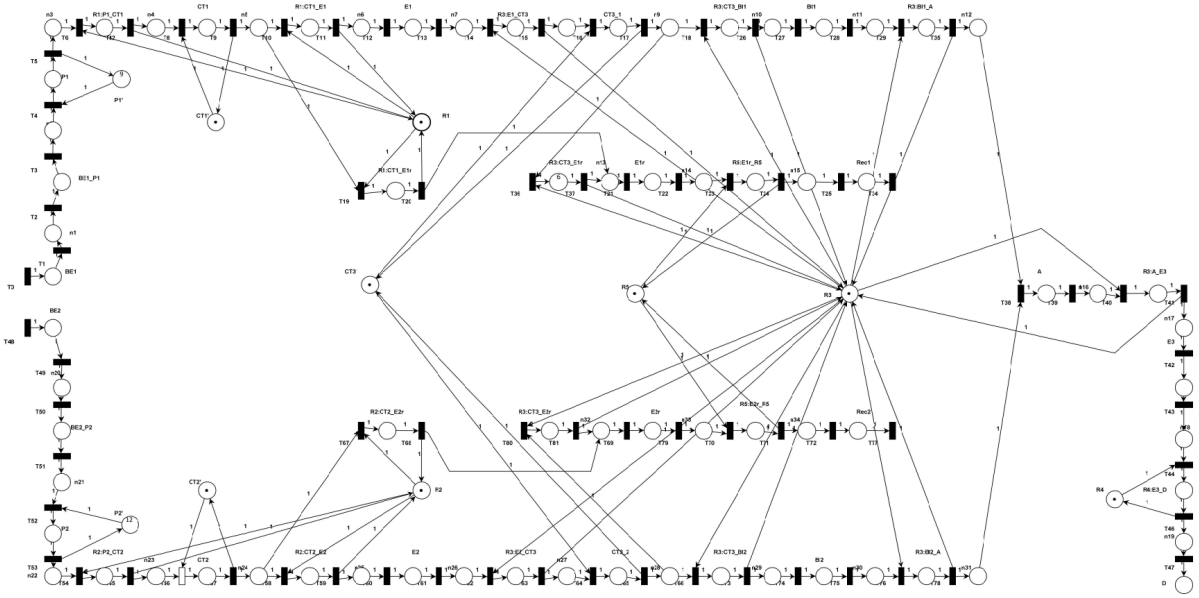

E System Inputs and Outputs

The inputs and outputs related to each activity are listed in the Figures 6 and 7. In order to make the analysis more organized, the term "activities" was divided into "tasks" and "movements".

Figure 6 - Inputs and outputs related to the activities.

Tasks	Inputs	Outputs
BE1: Arrival of metallic filament at Entrance Buffer 1	BE1_OK: Metallic filament available	-
BE2: Arrival of metallic powder at Entrance Buffer 2	BE2_OK: Metallic powder available	-
BE1_P1: Loading into Printer 1	BE1_P1_OK: Filament loaded into Printer 1	BE1_P1_load: Loads filament
BE2_P2: Loading into Printer 2	BE2_P2_OK: Powder loaded into Printer 2	BE2_P2_load: Loads powder
P1: Printing of combustion chamber by Printer 1	P1_OK: Printer 1 completed printing	P1_Proc: Printer performs printing
P2: Printing of turbopump by Printer 2	P2_OK: Printer 2 completed printing	P2_Proc: Printer performs printing
CT1: Inspection on Computerized Tomography Equipment 1	CT1_OK: Tomograph completed inspection	CT1_Proc: Tomograph performs inspection
CT2: Inspection on Computerized Tomography Equipment 2	CT2_OK: Tomograph completed inspection	CT2_Proc: Tomograph performs inspection
CT3_1: Inspection of the chamber on Computerized Tomography Equipment 3	CT3_1_OK: Tomograph completed inspection for chamber	CT3_1_Proc: Tomograph performs inspection
CT3_2: Inspection of the turbopump on Computerized Tomography Equipment 3	CT3_2_OK: Tomograph completed inspection for turbopump	CT3_2_Proc: Tomograph performs inspection
BI1: Arrival of combustion chambers at Intermediate Buffer 1	BI1_OK: Chamber in the buffer	-
BI2: Arrival of turbopumps at Intermediate Buffer 2	BI2_OK: Turbopump in the buffer	-
A: Assembly of parts	A_OK: Assembly completed	A_Proc: Assembly to be performed
D: Storage of parts in the warehouse	D_OK: Piece stored in the warehouse	-
Rec1: Arrival of defective chambers at the recycling bay	Rec1_OK: Defective chamber arrived in recycling bay	-
Rec2: Arrival of defective turbopumps at the recycling bay	Rec2_OK: Defective turbopump arrived in recycling bay	-

Figure 7 - Inputs and outputs related to the movements.

Movements	Inputs	Outputs
R1:P1_CT1: Movement P1>CT1 through robot 1	R1:P1_CT1_OK: Robot completed movement	R1:P1_CT1_Tr: Robot performs transportation
R1:CT1_E1: Movement CT1>E1 through robot 1	R1:CT1_E1_OK: Robot completed movement	R1:CT1_E1_Tr: Robot performs transportation
R1:CT1_E1r: Movement CT1>E1r through robot 1	R1:CT1_E1r_OK: Robot completed movement	R1:CT1_E1r_Tr: Robot performs transportation
R2:P2_CT2: Movement P2>CT2 through robot 1	R2:P2_CT2_OK: Robot completed movement	R2:P2_CT2_Tr: Robot performs transportation
R2:CT2_E2: Movement CT2>E2 through robot 1	R2:CT2_E2_OK: Robot completed movement	R2:CT2_E2_Tr: Robot performs transportation
R2:CT2_E2r: Movement CT2>E2r through robot 1	R2:CT2_E2r_OK: Robot completed movement	R2:CT2_E2r_Tr: Robot performs transportation
R3:E1_CT3: Movement E1>CT3 through robot 3	R3:E1_CT3_OK: Robot completed movement	R3:E1_CT3_Tr: Robot performs transportation
R3:CT3_BI1: Movement CT3>BI1 through robot 3	R3:CT3_BI1_OK: Robot completed movement	R3:CT3_BI1_Tr: Robot performs transportation
R3:CT3_E1r: Movement CT3>E1r through robot 3	R3:CT3_E1r_OK: Robot completed movement	R3:CT3_E1r_Tr: Robot performs transportation
R3:BI1_A: Movement BI1>A through robot 3	R3:BI1_A_OK: Robot completed movement	R3:BI1_A_Tr: Robot performs transportation
R3:E2_CT3: Movement E2>CT3 through robot 3	R3:E2_CT3_OK: Robot completed movement	R3:E2_CT3_Tr: Robot performs transportation
R3:CT3_BI2: Movement CT3>BI2 through robot 3	R3:CT3_BI2_OK: Robot completed movement	R3:CT3_BI2_Tr: Robot performs transportation
R3:CT3_E2r: Movement CT3>E2r through robot 3	R3:CT3_E2r_OK: Robot completed movement	R3:CT3_E2r_Tr: Robot performs transportation
R3:BI2_A: Movement BI2>A through robot 3	R3:BI2_A_OK: Robot completed movement	R3:BI2_A_Tr: Robot performs transportation
R3:A_E3: Movement A>E3 through robot 3	R3:A_E3_OK: Robot completed movement	R3:A_E3_Tr: Robot performs transportation
R4:E3_D: Movement R3>D through robot 4	R4:E3_D_OK: Robot completed movement	R4:E3_D_Tr: Robot performs transportation
R5:E1r_R1: Movement E1r>R1 through robot 5	R5:E1r_R1_OK: Robot completed movement	R5:E1r_R1_Tr: Robot performs transportation
R5:E2r_R2: Movement E2r>R2 through robot 5	R5:E2r_R2_OK: Robot completed movement	R5:E2r_R2_Tr: Robot performs transportation
E1: Movement through conveyor belt 1	E1_OK: Arrival of the piece at the destination	-
E2: Movement through conveyor belt 2	E2_OK: Arrival of the piece at the destination	-
E3: Movement through conveyor belt 3	E3_OK: Arrival of the piece at the destination	-
E1r: Movement through conveyor belt 1r, to the recycling area	E1r_OK: Arrival of the piece at the destination	-
E2r: Movement through conveyor belt 2r, to the recycling area	E1r_OK: Arrival of the piece at the destination	-

F Representation of Data Flow with the External Environment

Finally, by combining the Petri net with the list of tasks, it is possible to generate a diagram that explicitly illustrates all activities in their correct sequence, the resources to be used and shared, as well as the data flow with the external environment.

Figure 8 - Legenda acima da Figure. {Legenda}

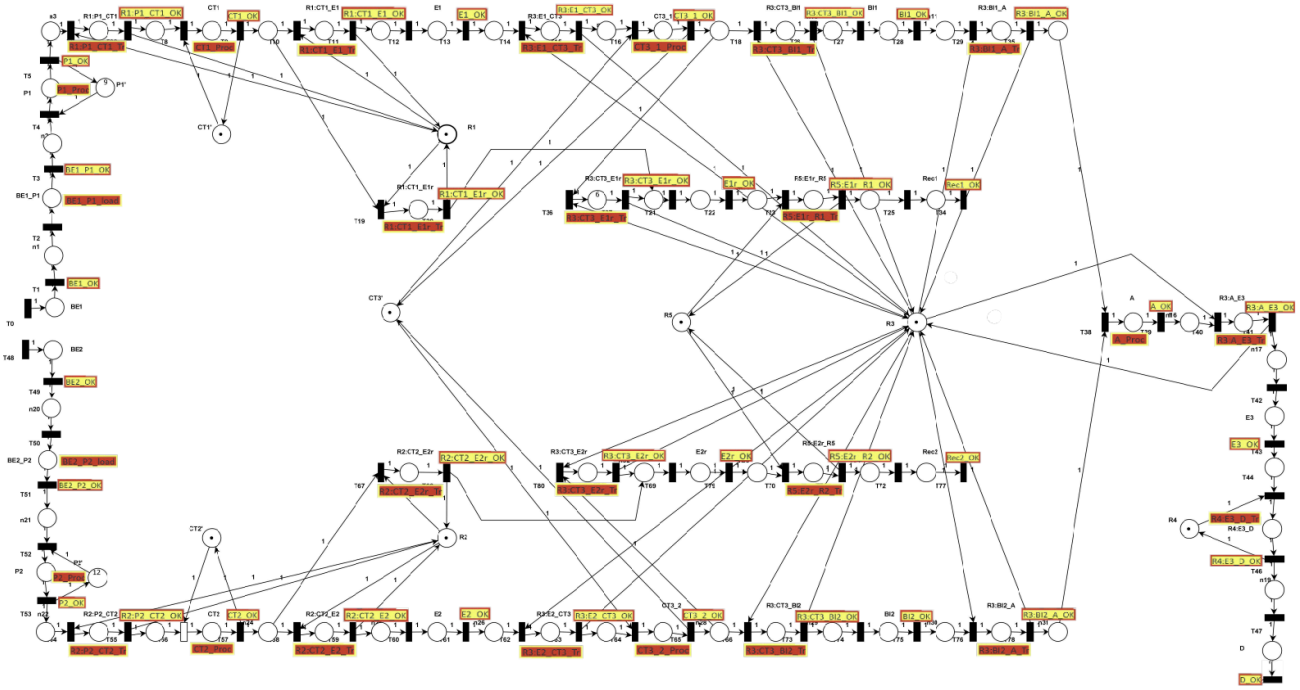

3.4 Programmable Logic Controllers (PLCs) programming

Programmable Logic Controllers (PLCs) play a pivotal role in industrial automation by providing a flexible and efficient means of controlling various processes and machinery. These digital devices are programmable, allowing engineers and technicians to create customized sequences, logic operations, and automation tasks. PLCs are widely used in manufacturing, assembly lines, and industrial processes, offering reliability, scalability, and ease of maintenance. Their ability to interface with sensors, actuators, and other control devices makes them indispensable for optimizing and streamlining complex operations in diverse industries.

Ladder Logic, a key component in industrial automation, simplifies control system programming through graphical symbols resembling relay logic. Widely used in Programmable Logic Controllers (PLCs), it facilitates the creation of intricate control sequences for efficient and precise automation.

A Ladder program was developed and can be found at Ladder Diagram.

4 Model Validation

In order to validate the construction of the model, it is essential to examine its respective properties. Thus, we can highlight them as liveness and safety, boundedness, reversibility, persistence, and fairness, as proposed by (CARDOSO, 1997). Below is the discussion concerning the network with its key characteristics.

4.1 Theoretical Validation

Boundedness and Safety: It is observed that regardless of the chosen place, the number of tokens will not exceed a finite quantity "k." Thus, the insertion of buffers and registers into the system remains limited to a finite amount, indicating a bounded network. Being a bounded network implies safety since boundedness ensures there will be no overflow in buffers or registers, irrespective of the sequence of events.

Liveness: Upon examining the Petri net of the system, the absence of deadlocks is evident, meaning there are no interlockings. Consequently, starting from position M(k0), it is possible to fire any other sequence of transitions through any sequence M(k). Therefore, most transitions exhibit L2-liveness as they allow the firing of a sequence up to k times. In contrast, transitions such as FT05, FT21, FT39, and FT43 display L1-liveness characteristics as they can be fired at least once depending on the firing sequence submitted.

Reversibility: Reversibility is asserted if, for any chosen place in the network, it can return to its initial state. Upon analyzing the Petri net of the system, it is evident that there are states that do not allow a return to the initial state. Thus, the network is considered non-reversible.

Persistence: Analyzing the network's characteristics reveals that the firing of one transition disables another. This behavior is observed in the transition from FT33 to FT21, where the firing of FT33 disables FT21. Therefore, it can be affirmed that the Petri net is non-persistent.

Fairness: Through simulation along with the Petri net, the behavior of the obtained firings demonstrates a "one-to-one" relationship, meaning there are equal weights of firings for each transition. Thus, for a global finite firing sequence σ, it can be characterized as unconditionally equal.

4.2 Simulation with *ProModel Software*

The model was implemented in the *ProModel* Discrete Event Simulator, from *ProModel Corporation,* following the guide provided on the company's website. Different situations were simulated to validate the model and assess the influence of different variables. The simulations were conducted for 1000 hours unless otherwise specified.

Figure 9 - Model of the system implemented in the ProModel software.

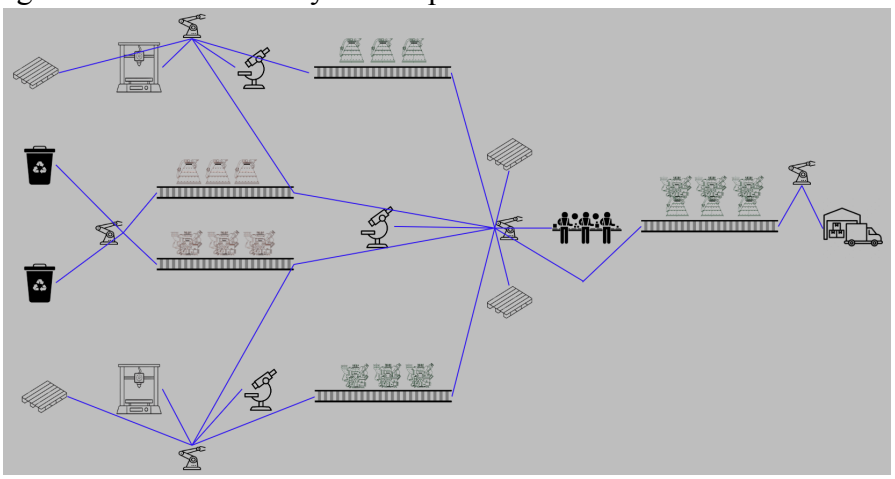

A simulation video can be found at Engine Factory Simulation.

Initially, the system was designed to operate on a time unit of 4 hours, as the assembly activity, which takes the least time, lasts 4 hours. Thus, since the printing of the combustion chamber takes 36 hours and the turbopump takes 48 hours, 9 P1 printers and 12 P2 printers were installed to produce one part every 4 hours. Computerized tomography, which is performed after the printing of each part, lasts 4 hours, so CT1 and CT2 tomographs operate practically uninterruptedly. Once approved, the combustion chamber moves to the oven, which has the E1 conveyor passing through its interior, so it operates continuously while transporting the part to the assembly bay. The same process occurs for the turbopump powder removal, which takes place on the E2 conveyor. In the assembly phase, both parts are again inspected by tomograph CT3, in a process that takes 2 hours for each part, totaling 4 hours of inspection. After assembly, which takes 4 hours, the engine is finally transported to the storage area (D) through the E3 conveyor.

In the described situation, disregarding the time for robot and E3 conveyor movement, neglecting possible variations in machine operation time, and considering a rejection rate of 0% in the tomographs, one can expect a production of 1 engine every 4 hours, thus producing 250 engines in a simulation of 1000 hours. In this case, since the Join operation, used to create the engine (Engine), maintains the attributes and name of the base entity, the combustion chamber (CC), the number of exits from engines must also be accounted for in the number of exits from chambers. Clearly, in reality the number of exits for chambers and turbopumps (TP) is indeed zero, as the rejection rate is 0%.

Figure 10 - Number of engines manufactured with 1000 hours of simulation.

Scoreboard

Name	Total Exits	Average Time In System (Hr)
CC	237.00	54.16
TP	0.00	0.00
Engine	237.00	54.16

As depicted in the figure, the production was 237 engines, which is lower than the expected value. This result is attributed to transient effects during the initial operation of the system, such as waiting for the first parts to be printed, inspected, post-processed, and inspected again before reaching the assembly bay. As a transient problem, its effect can be mitigated by increasing the simulation time, as illustrated in the figure.

Figure 11 - Number of engines manufactured with 10,000 hours of simulation.

Scoreboard

Name	Total Exits	Average Time In System (Hr)
CC	2,487.00	54.16
TP	0.00	0.00
Engine	2,487.00	54.16

Another point to be noted is the utilization of printers and tomographs, which is over 95%, not reaching 100% due to the aforementioned transient effects.

Figure 12 - Percentage of usage of printers and tomographs.

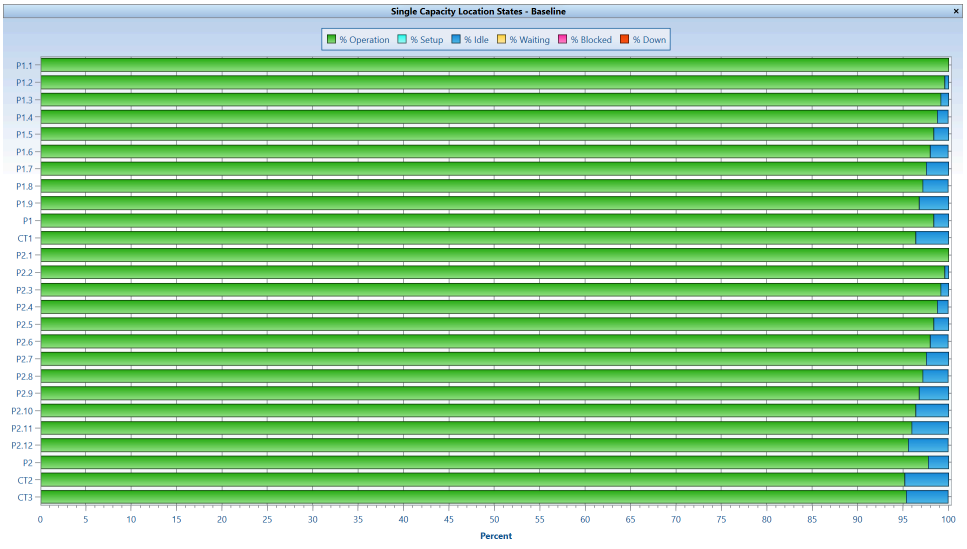

Furthermore, the utilization time of the robots is zero, as expected.

Figure 13 - Percentage of usage of the robots.

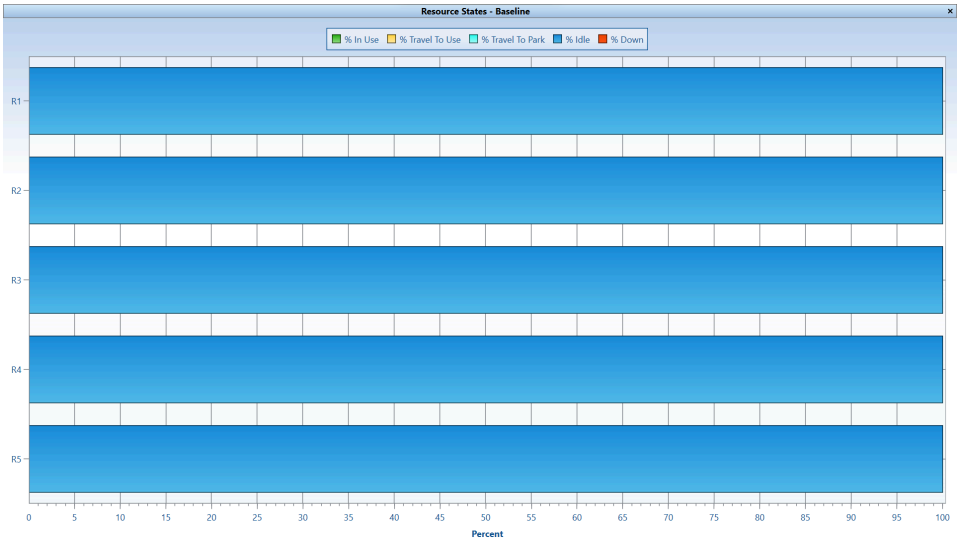

In order to make the simulation more realistic, the robot movement times were also taken into account, considering an average time of 1 minute when idle and 5 minutes when busy. Additionally, it was considered that conveyors E3, E1r, E2r, and E3r take about 30 minutes to transport the parts. A new simulation was executed. As expected, a lower output of engines is observed, with 197 units every 1000 hours.

Figure 14 - Number of engines manufactured with 1000 hours of simulation, considering the speed of movement of resources.

Scoreboard

Name	Total Exits	Average Time In System (Hr)
CC	198.00	133.91
TP	0.00	0.00
Engine	197.00	133.88

Furthermore, a decrease in printer utilization to around 88% can be observed, as expected, since their idle time will be higher due to the robot movement time.

Figure 15 - Percentage of printer and tomograph usage, considering the speed of resource movement.

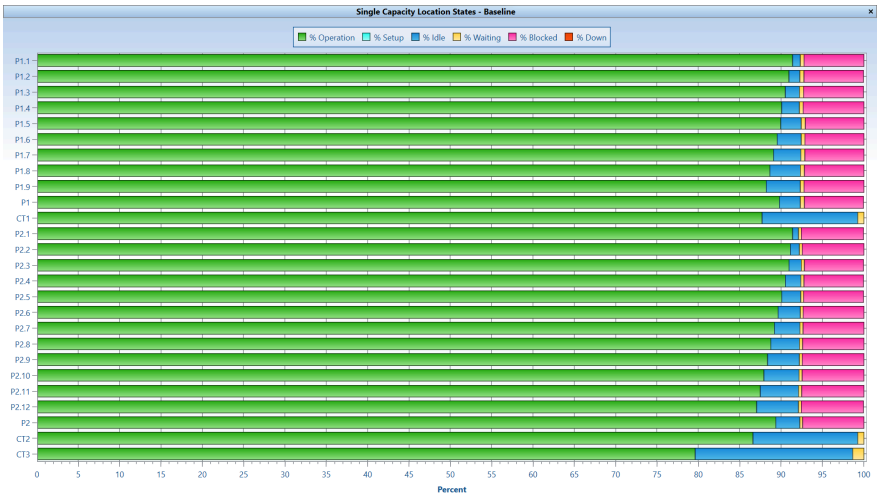

As expected, it can also be noted that the usage time of R3 is about twice that of R1 and R2, as it needs to handle a flow of parts twice as large. On the other hand, R4 is about one-third of R1 and R2 since, although the flow of parts is the same, R4 only needs to make one movement with each part, while R1 and R2 need to make three movements for each piece. Obviously, the usage time of R4 is still zero since no parts are being rejected.

Figure 16 - Percentage of robot usage, considering the speed of resource movement.

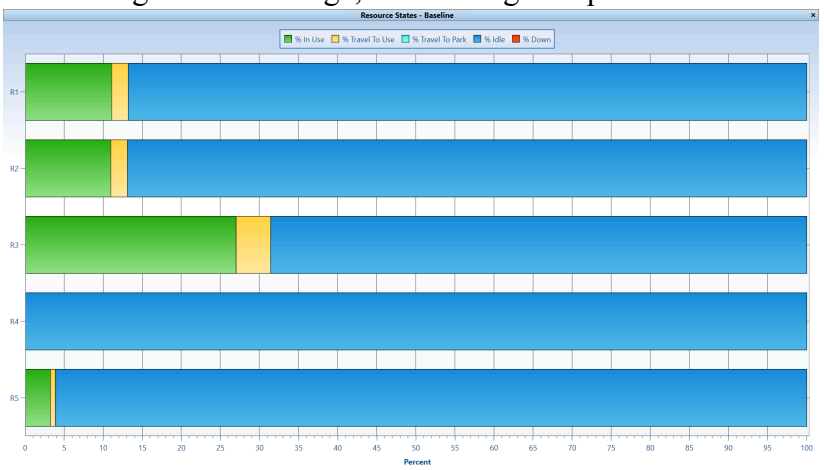

To make the model even closer to reality, a non-zero rejection rate of parts during their inspection by computerized tomography can be considered. A rejection rate of 10% for both parts in the first inspection, where most problems occur, and 5% in the second inspection were considered, resulting in a total global rejection rate of 14.5%, as confirmed in the figure.

Figure 17 - Number of engines manufactured with 1000 hours of simulation, considering the speed of resource movement and the reject rate of parts.

Scoreboard

Name	Total Exits	Average Time In System (Hr)
CC	224.00	96.46
TP	18.00	101.33
Engine	174.00	123.85

As expected, the use of printers and tomographs CT1 and CT2 did not decrease, but the use of tomograph CT3 dropped considerably since a smaller quantity of parts reaches it.

Figure 18 - Percentage of printer and tomograph usage, considering the speed of resource movement and the reject rate of parts.

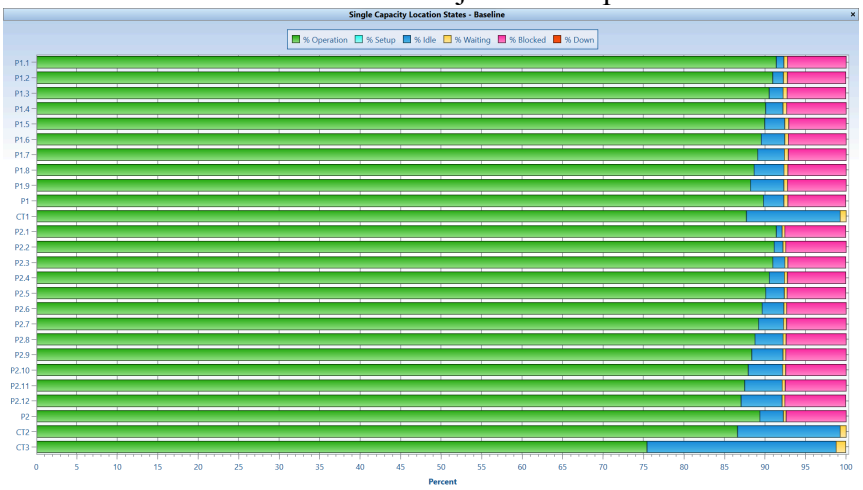

On the other hand, the use of R1 and R2 remained constant, while the use of R3 and R5 dropped slightly. The use of R4 is no longer zero.

Figure 19 - Percentage of robot usage, considering the speed of resource movement and the reject rate of parts.

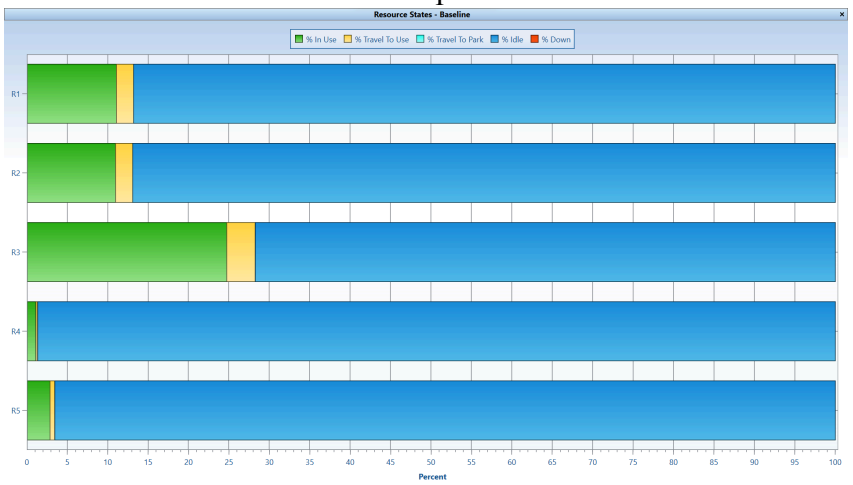

Once the resource movement time is not zero, one might consider reducing the number of printers to cut down the overall system costs, as they represent the most expensive machinery. Therefore, simulating with one less printer in each of the printing bays unexpectedly results in increased production.

Figure 20 - Number of engines produced with 1000h of simulation, considering the speed of resource movement, the reject rate of parts, and reducing one printer in each bay.

Scoreboard

Name	Total Exits	Average Time In System (Hr)
CC	217.00	110.59
TP	13.00	91.68
Engine	181.00	112.34

Regarding the use of printers and tomographs, the use of printers increased, and that of tomographs remained as expected and desired with the modification.

Figure 21 - Percentage of printer and tomograph usage, considering the speed of resource movement, reject rate of parts, and one less printer in each bay.

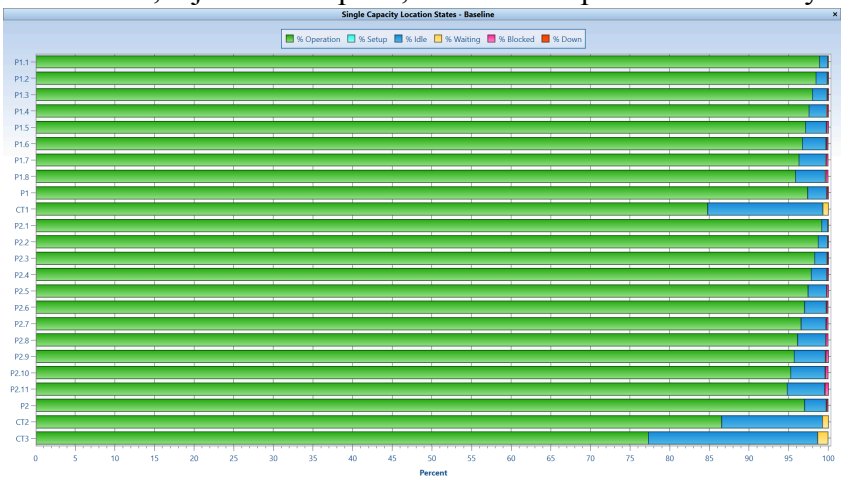

The use of robots remained approximately unchanged.

Figure 22 - Percentage of robot usage, considering the speed of resource movement, reject rate of parts, and one less printer in each bay.

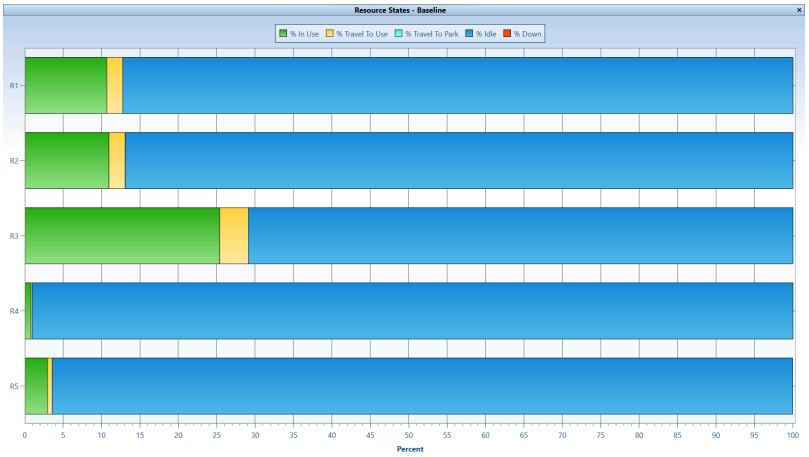

With a reduction of two printers per bay, there is a decrease in production, as expected.

Figure 23 - Number of engines produced with 1000h of simulation, considering the speed of resource movement, reject rate of parts, and two fewer printers in each bay.

Scoreboard

Name	Total Exits	Average Time In System (Hr)
CC	196.00	159.73
TP	24.00	126.40
Engine	158.00	142.26

Moreover, to make the model even more realistic, in the aforementioned simulations it was also considered that the duration of printing and inspection activities, as well as movements, follows a distribution, for example, normal, with a known standard deviation.

5 Conclusions

In this study, it was possible to observe that the methodology applied for the project was of utmost importance to have a clear view of the production process. The development of the Production Flow Schema, Petri Net, Ladder, and simulations in ProModel allowed for an understanding of how each stage of the project is interconnected, making it crucial. It is worth noting that the more information is inserted into the model, the closer it gets to real behavior.

This analysis is crucial for identifying potential bottlenecks in the production system, as well as predicting the propagation of failures, facilitating its improvement and the design of a more robust and efficient system.

With the present study, the aim to contribute to the rocket manufacturing sector, which is essential for human activities and has a promising growth potential.

ACKNOWLEDGMENTS

We acknowledge Professors Diolino José dos Santos Filho and Fabrício Junqueira for their guidance during the completion of this study.

REFERENCES

3D SYSTEMS. German Aerospace Center (DLR) Designs Liquid Rocket Engine Injector with 3D Systems. 2020. Retrieved from https://www.3dsystems.com/customer-stories/german-aerospace-center-dlr-designs-liquid-rocket-engine-injector-3d-systems

BAO, B., ZHOU, L., WANG, J., & XIAO, S. Application and challenges of additive manufacturing in the liquid rocket engines. 2022. SPIE-Intl Soc Optical Eng, 240.

BECK et al. Rocket Engine Thrust Chamber, Injector, and Turbopump. 2019.

BLAKEY-MILNER, B., GRADL, P., SNEDDEN, G., BROOKS, M., PITOT, J., LOPEZ, E., ... & PLESSIS, A. Metal additive manufacturing in aerospace: A review. Materials and Design, 2019, 209.

CARDOSO, J.; VALETTE, R. Redes de Petri. Florianópolis, 1997.

GRADL, P., MIRELES, O., & ANDREWS, N. Introduction to Additive Manufacturing for Propulsion Systems.

MORIYA, S., INOUE, T., SASAKI, M., NAKAMOTO, T., KIMURA, T., NOMURA, N., ... & MASUDA, I. Feasibility Study on Additive Manufacturing of Liquid Rocket Combustion Chamber. TRANSACTIONS OF THE JAPAN SOCIETY FOR AERONAUTICAL AND SPACE SCIENCES, AEROSPACE TECHNOLOGY JAPAN, 2020, 16(3), 261–266.

MIYAGI, P.E. Controle Programável: Fundamentos do Controle de Sistemas a Eventos Discretos. Brasil: Blucher, 1996, 206p.

REI, M. Rocket Engine Made by Additive Manufacturing. IHI Corporation, Tech. Rep, 2018.

SALMI, B. 3D-Printing a Rocket. IEEE Spectrum, 2019.

SOLLER, S., & ARIANE GROUP. Development of Liquid Rocket Engine Injectors Using Additive Manufacturing. 2015. Retrieved from https://www.researchgate.net/publication/280561310

SOLLER, S., BARATA, A., BEYER, S., DAHLHAUS, A., GUICHARD, D., HUMBERT, E., ... & ZEISS, W. Selective Laser Melting (Slm) Of Inconel 718 And Stainless Steel Injectors For Liquid Rocket Engines. 2016. Retrieved from https://www.researchgate.net/publication/303331194

YUSUF, S. M., CUTLER, S., & GAO, N. Review: The impact of metal additive manufacturing on the aerospace industry, 2019.

Eduardo Seiji Suguimoto Miyazato Ferrer is a Mechatronics Engineering student at the Polytechnic School of the University of São Paulo, holding a prior degree in Molecular Sciences, also from the University of São Paulo. He was a member of the motorsports and the rocket team, focusing on the design, simulation, manufacturing, and testing of power transmission systems, as well as solid and hybrid rocket engines. Currently, he is involved in research at the Combustion and Propulsion Laboratory of the National Institute for Space Research. Eduardo is deeply passionate about aerospace and automotive engineering, harboring a dream of contributing to humanity's return to the Moon and journey to Mars.

Jhonatan Ribeiro dos Santos is a Mechatronics Engineering student at the Polytechnic School of the University of São Paulo, earning a technical degree from SENAI. Noteworthy for his active involvement as a monitor in the "Noite com as Estrelas" project by the Institute of Astronomy, Geophysics, and Atmospheric Sciences (IAG) at USP, Jhonatan combines theoretical knowledge with practical experience. His commitment to community outreach and passion for mechatronics mirrors his dedication to academia. Inspired by the prospect of bridging technology and education, Jhonatan aspires to contribute significantly to the field as he advances in his academic journey.